KARL-FRANZENS-UNIVERSITÄT GRAZ
UNIVERSITY OF GRAZ

Cross-Validating and Interpreting Results of Magnetic Helicity Calculation Methods in Eruptive NOAA Active Region 10930

J. K. Thalmann[1], M. K. Georgoulis[2], Y. Liu[3], E. Pariat[4,5], G. Valori[6], S. Anfinogentov[7], F. Chen[8], Y. Guo[8], K. Moraitis[9], S. Yang[10]
(ISSI Team on Magntetic Helicity; http://www.issibern.ch/teams/magnetichelicity)
and
A. Mastrano[11]

[1]University of Graz, Institute of Physics/IGAM, Graz, Austria
[2]Research Center for Astronomy and Applied Mathematics of the Academy of Athens, Athens, Greece
[3]W.\ W.\ Hansen Experimental Physics Laboratory, Stanford, CA, USA
[4]Laboratoire de Physique des Plasmas (LPP), CNRS, Sorbonne Université, École polytechnique, Institut Polytechnique de Paris, Palaiseau, France
[5]LESIA, Observatoire de Paris, Université PSL, CNRS, Sorbonne Université, Université de Paris, Meudon, France
[6]Max-Planck-Institut für Sonnensystemforschung, Göttingen, Germany
[7]Institute of Solar-Terrestrial Physics, Irkutsk, Russia
[8]School of Astronomy and Space Science, Nanjing University, Nanjing, China
[9]Physics Department, University of Ioannina, Ioannina, Greece
[10]Key Laboratory of Solar Activity, National Astronomical Observatories, Chinese Academy of Sciences, Beijing, China
[11]Sydney Institute for Astronomy, School of Physics, University of Sydney, NSW, Australia

Session 2 - The Solar Atmosphere: Heating, Dynamics and Coupling
Poster ID #320
Preprint available at: https://arxiv.org/abs/2108.08525

FWF Der Wissenschaftsfonds.
INTERNATIONAL SPACE SCIENCE INSTITUTE

Context

Magnetic helicity: signed scalar quantity that numbers the structural complexity of a magnetic field.

$$\mathscr{H}_{\mathcal{V}} \equiv \int_{\mathcal{V}} (\boldsymbol{A} \cdot \boldsymbol{B}) \, \mathrm{dV} \quad \text{with} \quad \boldsymbol{B} = \nabla \times \boldsymbol{A} \quad \text{and} \quad \nabla \cdot \boldsymbol{B} = 0$$

To be gauge-invariant: $\boldsymbol{B} \cdot \hat{\boldsymbol{n}}|_{\partial\mathcal{V}} = 0$

→ Hardly achieved for coronal cases, since magnetic flux is continuously penetrating (from below the photosphere) and leaving (carried away by the solar wind) the coronal volume.

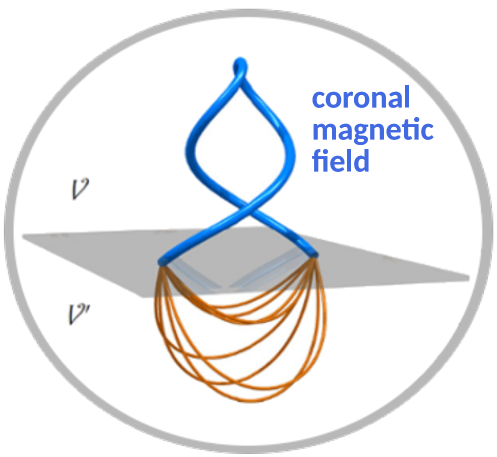

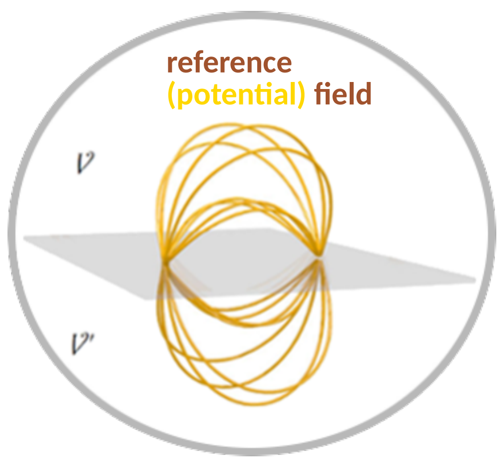

Relative helicity: $\mathscr{H}_{\mathcal{V}} \equiv \int_{\mathcal{V}} (\boldsymbol{A} + \boldsymbol{A}_{\mathrm{p}}) \cdot (\boldsymbol{B} - \boldsymbol{B}_{\mathrm{p}}) \, \mathrm{dV}$

(Berger & Field 1984; Finn & Antonsen 1985)

→ Formal closure of the magnetic flux is obtained by using the potential field $\boldsymbol{B}_{\mathrm{p}} = \nabla\varphi$, satisfying $(\hat{\boldsymbol{n}} \cdot \nabla\varphi)| = (\hat{\boldsymbol{n}} \cdot \boldsymbol{B})|$ on $\partial\mathcal{V}$.

→ Gauge-invariant, physically meaningful quantity.

Methods

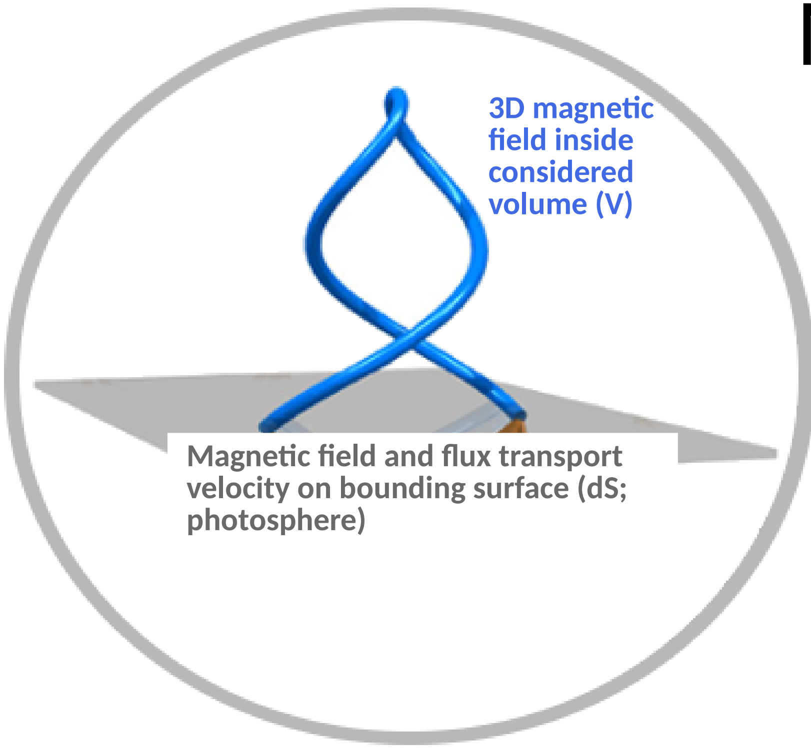

- Finite-volume methods (5):

→ Require 3D magnetic field inside V (this work: nonlinear force-free (NLFF) models).
→ Use either of two gauges: Coulomb (Thalmann et al. 2011; Yang et al. 2018) or DeVore (Valori et al. 2012; Moraitis et al. 2014) to compute the 3D vector potentials.
→ Provide instantaneous estimate of H_V from directly evaluating

$$\mathscr{H}_{\mathcal{V}} \equiv \int_{\mathcal{V}} (\boldsymbol{A} + \boldsymbol{A}_\mathrm{p}) \cdot (\boldsymbol{B} - \boldsymbol{B}_\mathrm{p}) \, \mathrm{dV}$$

- Connectivity-based method (1): (Georgoulis et al. 2012)

→ Requires magnetic field on dV
→ Relies on multi-polar partitioning of photospheric flux distribution to approximate the unknown coronal connectiviy in the form of a collection of force-free flux tubes ("skeletal" NLFF method based on a minimal connection-length principle).
→ Provides instantaneous estimate of H_V.

- Helicity-flux integration methods (2):

→ Require time evolution of magnetic field (B) and flux transport velocity (u) on dS.
→ This work: use the Coulomb gauge for vector potential.
→ Provide instantaneous estimate of dH_V/dt and by evaluating

$$\frac{\mathrm{d}\mathscr{H}_{\mathcal{V}}}{\mathrm{d}t} = -2 \int_{\partial\mathcal{V}} (\boldsymbol{A}_\mathrm{p} \cdot \boldsymbol{u}) \, B_\mathrm{n} \, \mathrm{dS}$$ (Liu & Schuck, 2012)

or

$$\frac{\mathrm{d}\mathscr{H}_{\mathcal{V}}}{\mathrm{d}t} = \int_{\partial\mathcal{V}} \int_{\partial\mathcal{V}} \frac{B_\mathrm{n} B'_\mathrm{n} ((\boldsymbol{u} - \boldsymbol{u}') \times (\boldsymbol{x} - \boldsymbol{x}'))_n}{2\pi (\boldsymbol{x} - \boldsymbol{x}')^2} \, \mathrm{dS} \, \mathrm{dS}'.$$ (Pariat et al. 2005)

→ Provide measure of accumulated helicity (H_{acc}) by time integration (reference helicity level needed for comparison with H_V).

Scope

Pioneering benchmarking works:

(Valori et al. 2016, Guo et al. 2017, Pariat et al. 2021)

Based on physically meaningful test magnetic fields (synthesized/idealized data):

→ **Finite-volume methods:**
Mutually agree to within ~3%.

→ **Connectivity-based method:**
Agree with finite-volume estimates to within ~10% at best.

→ **Helicity-flux integration methods:**
Mutually agree to within ~1%.
Agree with finite-volume estimates to within ~20% at best.

Objective 1:
Verify consistency of methods for observation-based data.

Earlier works on evolution of target AR (10930):

(Zhang et al. 2008, Park et al. 2010, Ravindra et al. 2011)

Based on observation-based data:

→ **Finite-volume helicity:**
On the order of 10^{43} Mx^2, negative in sign.

→ **Helicity-flux:**
Predominantly right-handed (positive) rate of helicity injection, followed by transition to strong negative values.
Reversal of sign in helicity flux during impluslive phase of X-flare.
Insignifant contribution to coronal helicity.
Lack of agreement of H_acc with respect to finite-volume estimate.

Objective 2:
Provide encompassing physical insight on active region evolution, in this case NOAA AR 10930.

Data

Table A1. Data sources and preparation for $\mathrm{CFIT_{sc}}$ modeling and the application of the different helicity computation methods. Indicated from left to right are the instances or time range, where applicable, of data coverage, the number of snapshots used within the covered time range, the data source, disambiguation method (where applicable; otherwise a cross '×' is used), the plate scale, the indication of the covered area on the solar disk in Fig. 1 (for data other than on December 11, a cross '×' is used) and the location of detailed data description in the main document.

Time (range) (UT)	No. of snapshots	Data source	Disambiguation method	Plate scale (arcsec)	Covered area as outlined in Fig. 1
$\mathrm{CFIT_{sc}}$ NLFF modeling					
Dec 11 17:00	1	SOT-SP[a]	NPFC[b]	0.66	magenta
Dec 12 20:30	1	SOT-SP[a]	ME[c]	0.63	×
Dec 13 04:30	1	SOT-SP[a]	ME[c]	0.63	×
FV helicity computations					
Dec 11 17:00	1	$\mathrm{CFIT_{sc}}$ $\boldsymbol{B}$	×	0.66	magenta
Dec 12 20:30	1	$\mathrm{CFIT_{sc}}$ $\boldsymbol{B}$	×	0.63	×
Dec 13 04:30	1	$\mathrm{CFIT_{sc}}$ $\boldsymbol{B}$	×	0.63	×
$\mathrm{CB_{FF}}$ helicity computation					
Dec 11 17:00	1	$\mathrm{CFIT_{sc}}$ $\boldsymbol{B}$ at $z=0$	×	0.66	magenta
Dec 12 20:30	1	$\mathrm{CFIT_{sc}}$ $\boldsymbol{B}$ at $z=0$	×	0.63	×
Dec 13 04:30	1	$\mathrm{CFIT_{sc}}$ $\boldsymbol{B}$ at $z=0$	×	0.63	×
$\mathrm{CB_{SP}}$ helcity computation					
Dec 11 03:10 – Dec 13 16:21	16	SOT-SP B_z	NPFC[b]	0.31	yellow
FI helcity flux computation					
Dec 11 12:09 – Dec 13 12:59	1150	SOT-NFI[d] B_{los}	×	0.15	green

[a] https://csac.hao.ucar.edu/sp_data.php
[b] Non-Potential magnetic Field Calculation (NPFC) method (Georgoulis 2005; Metcalf et al. 2006)
[c] Minimum-energy (ME) method (Metcalf 1994; Metcalf et al. 2006)
[d] Ichimoto & Hinode/SOT Team (2008)
[e] For December 11 data only

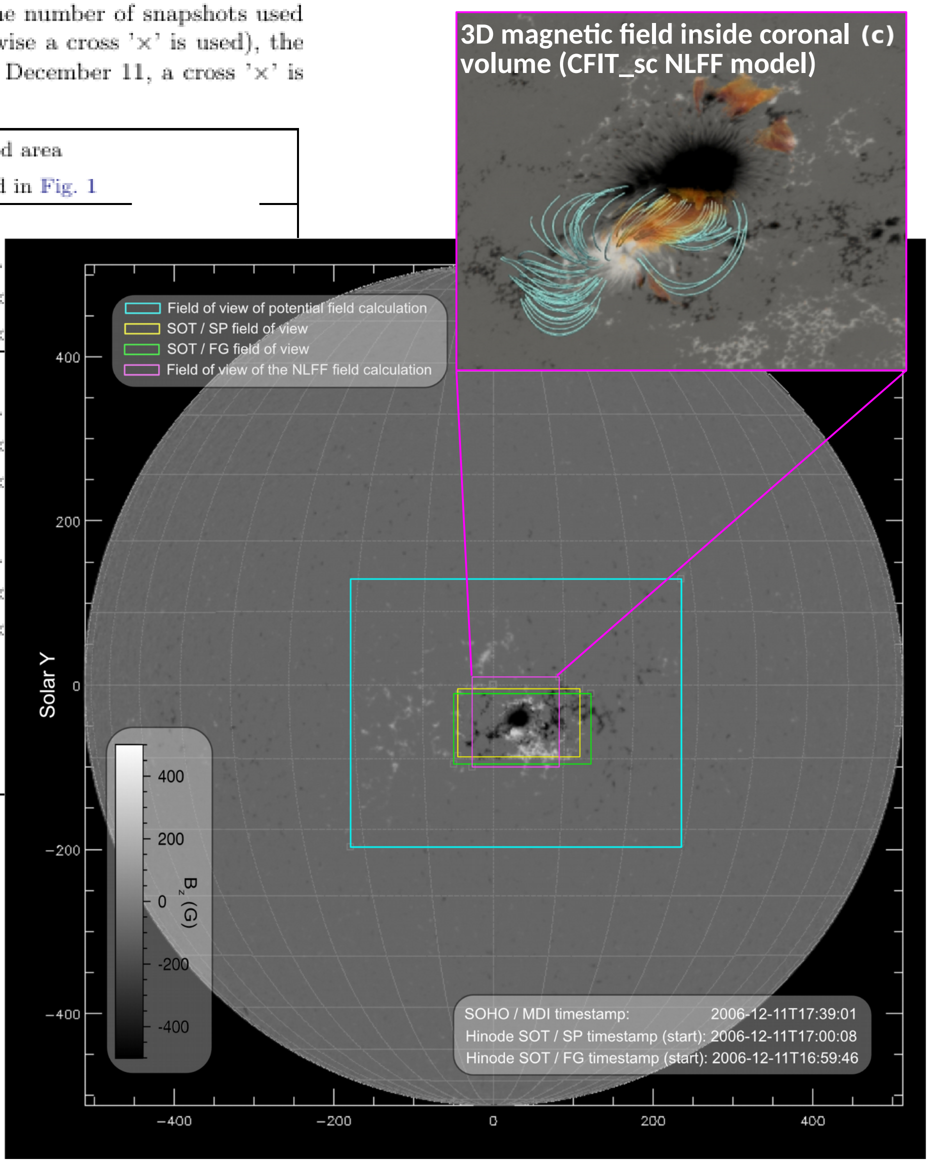

Results

Verify consistency of methods for observation-based data (Objective 1)

This work:
(Thalmann et al. 2021)

Based on observation-based data (NLFF modeling):

→ **Finite-volume methods:**
Mutually agree to within ~10%.

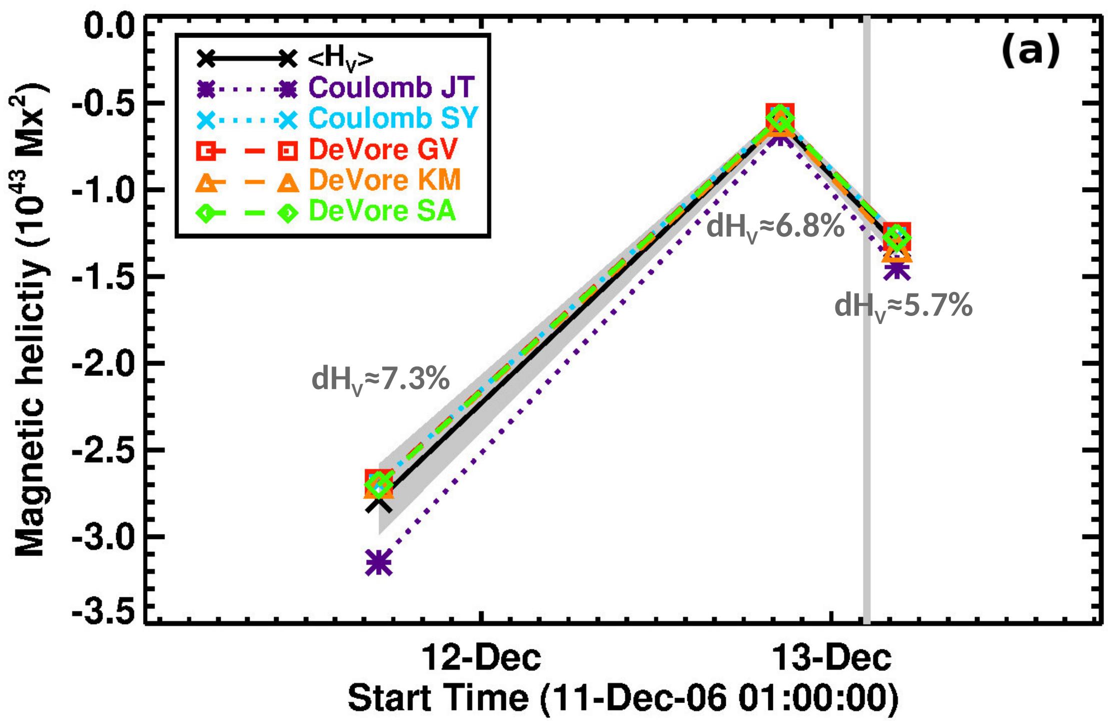

Results

Verify consistency of methods for observation-based data (Objective 1)

This work:
(Thalmann et al. 2021)

Based on observation-based data (SOT-SP data and NLFF modeling):

→ **Connectivity-based method:**
Agrees with finite-volume estimates to within ~30%.
Recovers same overall (negative) sign of coronal helicity.
Overall agreement regarding recovered time trends.
→ **Remarkable, given the very different methods!**

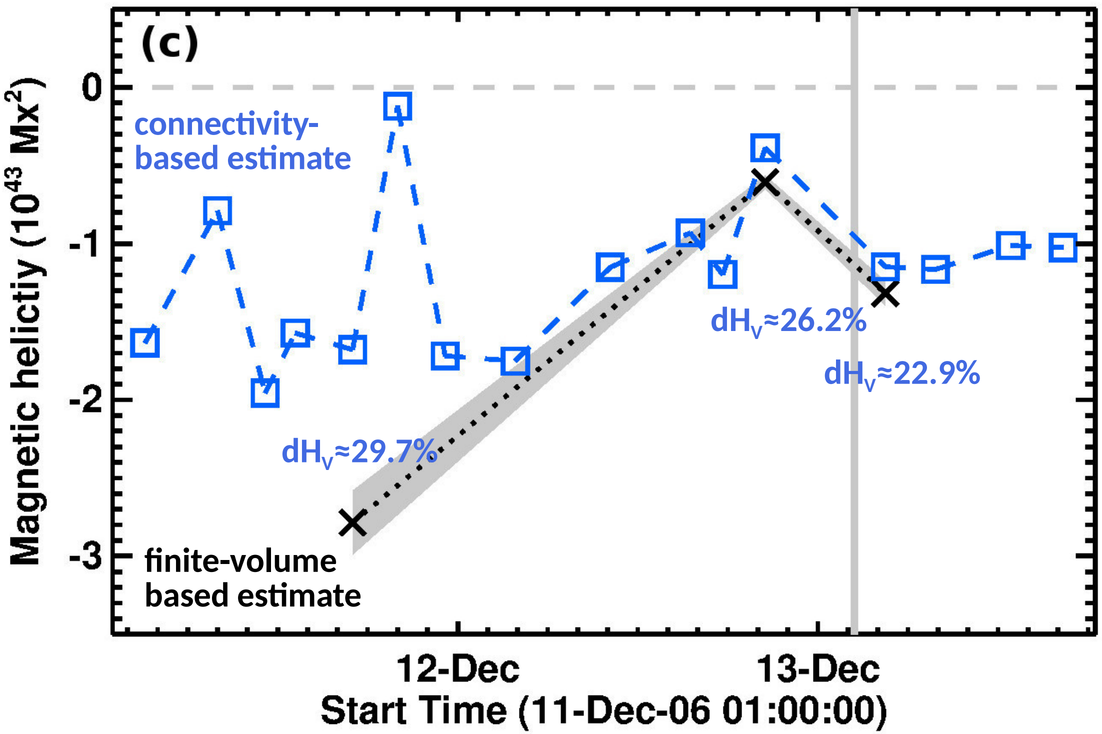

Results

Verify consistency of methods for observation-based data (Objective 1)

This work:
(Thalmann et al. 2021)

Based on observation-based data (SOT-SP and SOT-NFI data and NLFF modeling):

→ **Helicity-flux integration methods:**
Mutually agree to within ~5% (based on best-effort calibrated data).
Mutually agree on H_acc to within ~8%.
Overall agreement with finite-volume estimates regarding the predominant sign and magnitude of helicity.
→ **Remarkable, given that only helicity flux is captured!**
Loose to weak agreement of absolute values.
→ Known lack of correspondence!

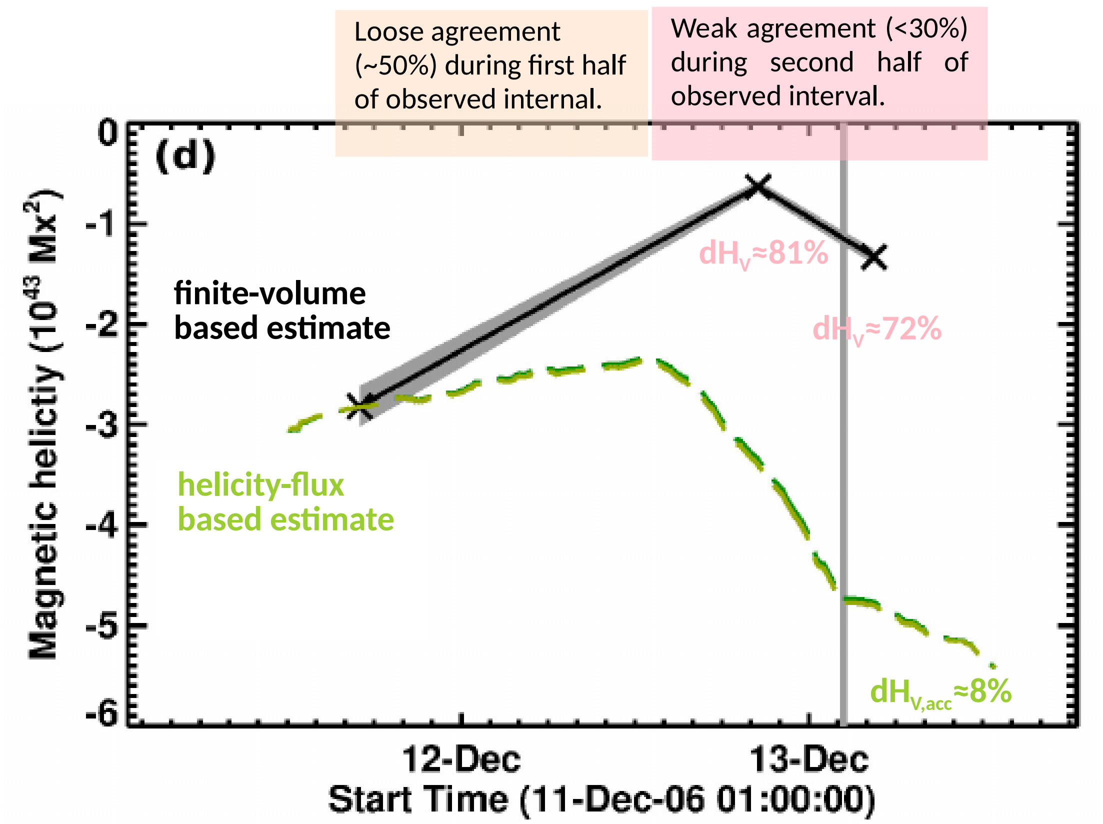

Summary

Verify consistency of methods for observation-based data (Objective 1)

Pioneering benchmarking works:

(Valori et al. 2016, Guo et al. 2017, Pariat et al. 2021)

Based on physically meaningful synthesized/idealized data:

→ **Finite-volume methods:**
Mutually agree to within ~3%.

→ **Connectivity-based method:**
Agree with finite-volume estimates to within ~10% at best.

→ **Helicity-flux integration methods:**
Mutually agree to within ~1%.
Agreement with finite-volume estimates (sign and magnitude of H_{acc} and H_v).

Agreement between absolute estimates (to within ~20% at best, during non-eruptive phase).

This work:

(Thalmann et al. 2021)

Based on observation-based data (SOT-SP and SOT-NFI data and NLFF modeling):

→ **Close correspondence of finite-volume methods:**
Mutual agreeement on helicity values to within ~10%.

→ **Connectivity-based method:**
Agreement with finite-volume estimates (predominant sign of helicity, magnitude to within ~30%, and time trend)
→ Remarkable, given the very different methods!
Connectivity-based results identify contributions of different handeness, yet are dependent input data.

→ **Helicity-flux integration methods:**
Mutual agreement to within ~8% (~5%) in (accumulated) helicity flux.
Overall agreement with finite-volume estimates (sign and magnitude of H_{acc} and H_v).
→ Remarkable, given that only helicity flux is captured.
Loose to weak agreement of absolute values.
→ Reference point for H_{acc} needed to complete evolutionary picture.
→ (Known) Lack of correspondence.

Thereby completing and verifying the findings of pioneering benchmarking works by Valori et al. (2016) and Pariat et al. (2021; forthcoming).

Results

Provide encompassing physical insight on NOAA 10930 (Objective 2)

This work:
(Thalmann et al. 2021)

→ **Dominant left-handed contribution to coronal helicity.**
Consistent with configuration of overall negative helicity.

→ **Co-temporal weak increase of right-handed contribution.**
Suggests emergence of oppositely helical structure (consistent with positive helicity flux) into pre-existing field.
Agreement with Inoue et al. (2012).

→ **Decrease of coronal helicty during Dec 11 & 12.**
Agreement with Park et al. (2010) & Georgoulis et al. (2012).

→ **Accumulation of positive helicity in active-region corona.**
Consistent with positive helicity flux and contributes markedly to coronal helicity budget.
Contrasting findings of Zang et al. (2008), Park et al. (2010).

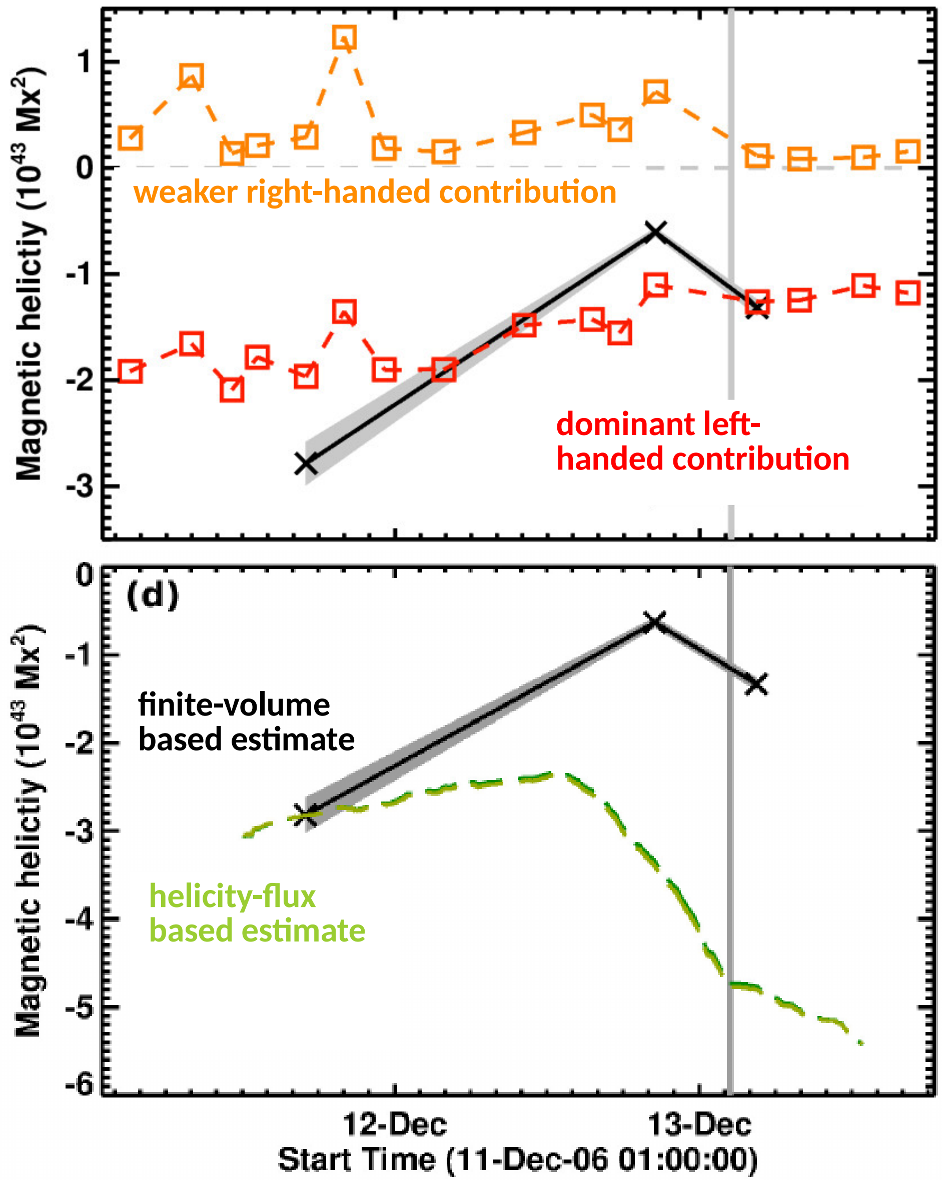

Results

Provide encompassing physical insight on NOAA 10930 (Objective 2)

This work:

(Thalmann et al. 2021)

→ **Photospheric helicity flux considerably different than in earlier studies** (one order of magnitude larger compared to Zhang et al. 2008, Park et al. 2010).

→ **Unphysical sign reversal in helicity flux during impulsive phase of X-flare.**
Contrasts earlier interpretations of rapid emergence of opposite helical field (e.g., Zhang et al. 2008; Park et al. 2010; Ravindra et al. 2011).

→ **Challenge of proper data callibration!**

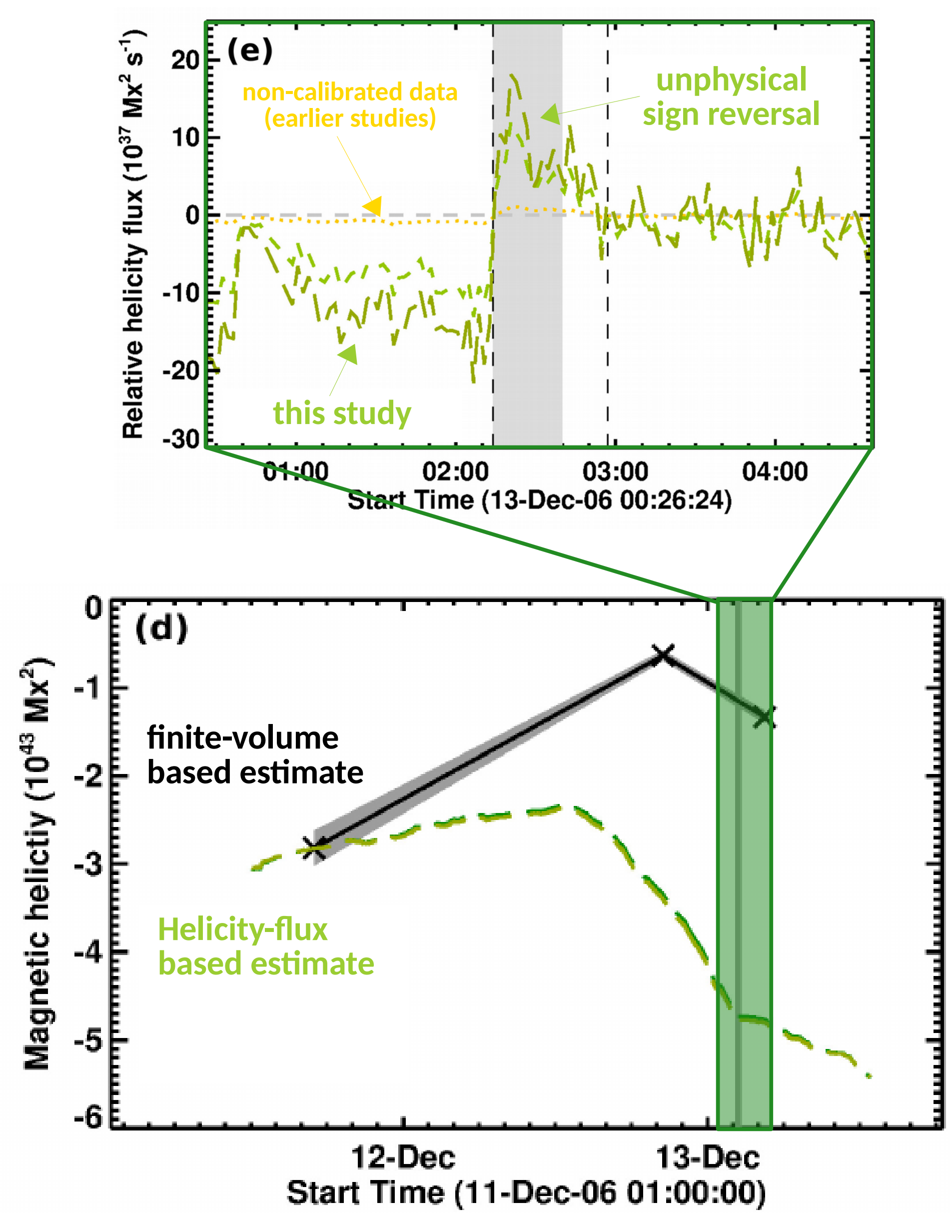

Summary

Provide encompassing physical insight on NOAA 10930 (Objective 2)

Earlier works on evolution of target AR (10930):

(Zhang et al. 2008, Park et al. 2010, Ravindra et al. 2011, Georgoulis et al. 2012, Inoue et al. 2012)

→ Finite-volume helicity (overall evolution):
On the order of 10^{43} Mx^2, negative in sign.
AR magnetic field predominantly negatively twisted.
Formation of positively-twisted field prior to flare onset.

→ Finite-volume helicity (flare-related changes):
Ejection of magnetic structure oppositely helical with respect to pre-existing field.

→ Helicity-flux (overall evolution):
Predominantly right-handed (positive) rate of helicity injection, followed by transition to strong negative values (~10^{36} Mx^2s^{-1}).

→ Relative contribution of helicity flux:
H_{acc} (10^{41} Mx^2) represetns a minor contribution to coronal helicity.

→ Helicity-flux (flare-related changes):
Reversal of sign in helicity flux during implusive phase of X-flare.
Insignifant contribution to coronal helicity.

This work:

(Thalmann et al. 2021)

→ Finite-volume helicity:
On the order of 10^{43} Mx^2, negative in sign. → Consistent.
From CB method: Dominant left-handed contribution. Co-temporal weak increase of right-handed contribution, suggesting emergence of oppositely helical structure. → Consistent.

→ Finite-volume helicity (flare-related changes):
Ejection of magnetic structure oppositely helical with respect to pre-existing field. → Consistent.

→ Helicity-flux (overall evolution):
Consistent time evolution, yet an order of magnitude higher (~10^{37} Mx^2s^{-1}, based on best-effort calibration of data).
→ Earlier findings only reproduced using non-calibrated data.

→ Relative contribution of helicity flux:
H_{acc} (10^{42} Mx^2) represetns a considerable contribution to coronal helicity budget.

→ Helicity-flux (flare-related changes):
Spurious signals in helicity flux when based on non-calibrated data.
→ Questinable interpretation as impulsive emergence of oppositely helical structure in previous works.

Thereby highliting the intricacies and difficulties of interpreting a complexity-ridden coronal evolution.

References

Berger, M. A., & Field, G. B., 1984, J. of Fluid Mechanics, 147, 133, doi: 10.1017/S0022112084002019

Finn, J. M., & Antonsen, T. M., 1985, Comm. Plasma Phys. Control. Fusion, 9, 111

Georgoulis, M. K., Tziotziou, K., & Raouafi, N.-E., 2012, The Astrophys. J., 759, 1, doi 10.1088/0004-637X/759/1/1

Guo, Y., Pariat, E., Valori, G., et al., 2017, The Astrophys. J., 840, 40, doi: 10.3847/1538-4357/aa6aa8

Inoue, S., Shiota, D., Yamamoto, T. T., et al., 2012, The Astrophys. J., 760, 17, doi: 10.1088/0004-637X/760/1/17

Liu, Y., & Schuck, P. W., 2012, The Astrophysical J., 761, 105, doi 10.1088/0004-637X/761/2/105

Moraitis, K., Tziotziou, K., Georgoulis, M. K., & Archontis, V., 2014, Solar Physics, 289, 4453, doi: 10.1007/s11207-014-0590-y

Pariat, E., Demoulin, P., & Berger, M. A., 2005, Astronomy & Astrophysics, 439, 1191, doi: 10.1051/0004-6361:20052663

Pariat, E., Valori, G., Anfinogentov, S., et al., 2021, Space Science Rev., in preparation

Park, S.-H., Chae, J., Jing, J., Tan, C., & Wang, H., 2010, The Astrophys. J., 720, 1102, doi: 10.1088/0004-637X/720/2/1102

Ravindra, B., Venkatakrishnan, P., Tiwari, S. K., & Bhattacharyya, R., 2011, The Astrophys. J., 740, 19, doi: 10.1088/0004-637X/740/1/19

Thalmann, J. K., Inhester, B., & Wiegelmann, T., 2011, Solar Physics, 272, 243, doi: 10.1007/s11207-011-9826-2

Thalmann, J. K., Georgoulis, M. K., Liu, Y., et al., 2021, eprint arXiv:2108.08525, accepted for publication in The Astrophysical J.

Valori, G., Demoulin, P., & Pariat, E., 2012, Solar Physics, 278, 347, doi: 10.1007/s11207-012-9951-6

Valori, G., Pariat, E., Anfinogentov, S., et al., 2016, Space Science Rev., 201, 147, doi: 10.1007/s11214-016-0299-3

Yang, S., Büchner, J., Skala, J., & Zhang, H., 2018, Astronomy & Astrophysics, 613, A27, doi: 10.1051/0004-6361/201628108

Zhang, Y., Tan, B., & Yan, Y., 2008, The Astrophys. J. Lett., 682, L133, doi: 10.1086/591027